Available online at www.sciencedirect.com
ScienceDirect
Journal of Catalysis 242 (2006) 340–348
JOURNAL OF CATALYSIS
www.elsevier.com/locate/jcat

Carbon incorporation during ethene oxidation on Pd(111) studied by in situ X-ray photoelectron spectroscopy at 2×10^{-3} mbar

Harald Gabasch [a,d], Evgueni Kleimenov [a], Detre Teschner [a], Spiros Zafeiratos [a], Michael Hävecker [a], Axel Knop-Gericke [a], Robert Schlögl [a], Dmitry Zemlyanov [b,c], Balazs Aszalos-Kiss [b], Konrad Hayek [d], Bernhard Klötzer [d,*]

[a] *Abteilung Anorganische Chemie, Fritz-Haber-Institut der Max-Planck-Gesellschaft, Faradayweg 4–6, D-14195 Berlin, Germany*
[b] *Materials and Surface Science Institute and Physics Department, University of Limerick, Limerick, Ireland*
[c] *Purdue University, Birck Nanotechnology Center, 1205 West State Street, West Lafayette, IN 47907-2057, USA*
[d] *Institut für Physikalische Chemie, Universität Innsbruck, Innrain 52A, A-6020 Innsbruck, Austria*

Received 3 May 2006; revised 21 June 2006; accepted 25 June 2006

Available online 4 August 2006

Abstract

The oxidation of ethene on the Pd(111) surface was studied in the temperature range of 330–923 K by in situ XPS and mass spectrometry during both heating and cooling in a reaction mixture of 5×10^{-4} mbar C_2H_4 and 1.5×10^{-3} mbar O_2. Carbon-containing surface species were found to be strongly predominant over oxygen species within the whole temperature range, despite the excess of oxygen in the gas phase. Diffusion of carbon into the palladium bulk started at 480 K, leading to the appearance of an electronically altered, dissolved carbon phase with a C1s binding energy of 284.45 eV at ∼500 K, which extended over several layers in the near-surface region and was stable up to ∼650 K. This spectroscopic trend was clearly related to a pronounced shift of catalytic selectivity toward CO. Above 660 K, the dissolved carbon species decomposed, and the reaction occurred on an adsorbate-depleted Pd metal surface, with CO as the main product. During the cooling ramp, the same near-surface carbon modification formed at a 70-degree-lower threshold temperature, inducing pronounced hysteresis of the catalytic selectivity.

Keywords: Palladium; Pd(111); Ethene oxidation; High pressure in situ XPS; Subsurface carbon; Dissolved carbon; Temperature-programmed reaction; Kinetic hysteresis

1. Introduction

The catalytic properties of palladium are known to depend strongly depend on its oxidation state. On the one hand, dispersed palladium metal is an important catalyst for hydrocarbon (in particular methane) combustion [1,2]. In case of methane oxidation (e.g., on alumina-supported Pd), the catalytic activity of Pd is associated with the kinetic hysteresis between formation and decay of the highly active PdO phase [3,4]. On the other hand, palladium-containing supported catalysts are also frequently used in the selective oxidation of hydrocarbons, for example, of ethene to acetaldehyde or to acetic acid [5–7] and of ethene plus acetic acid to vinyl acetate [8–11]. For these processes, the catalytic importance of carbon residing in the subsurface region of a highly reduced state of the catalysts has already been recognized [5,10,12]. For unsupported Pd, several modifications of the surface and the near-surface region have been reported in the literature, including the formation of a well-ordered hydride strongly promoting, say, ethene hydrogenation [13], and a solid solution of carbon formed near the Pd surface by different carbon-containing gases [14–16].

The main problem of previous ex situ studies is, of course, the stability of intermediate reactive species. Most of these species are metastable and may exist only under certain reaction conditions. As predicted by theoretical calculations of oxygen subsurface migration [17,18], a certain chemical potential of gas-phase oxygen is needed to establish a supersaturation of adsorbed oxygen on the surface, sufficient to stabilize the "dissolved" oxygen atoms beyond the first atomic layer, which

* Corresponding author. Fax: +43 512 507 2925.
E-mail address: bernhard.kloetzer@uibk.ac.at (B. Klötzer).

0021-9517/$ – see front matter
doi:10.1016/j.jcat.2006.06.022

are energetically less favorable than surface-adsorbed O-atoms. For carbon, the situation appears to be different. As has been revealed experimentally in our previous work and also substantiated by DFT calculations [18,19], the adsorbed carbon atoms need to overcome an activation barrier of 107 kJ/mol to pass the surface Pd layer (59–78 kJ/mol according to recent theory work [18]), but then become energetically stabilized in the subsurface or bulk dissolved state [18,20,21]. The activation barrier for C migration inside the bulk is considerably lower, at 65 kJ/mol [20]. Therefore, the amount of carbon expected within the first atomic layers will depend strongly on temperature, pressure, and time. In our previous UHV work, it was possible to quantify the irreversible rate of carbon uptake resulting from ethane dissociation through the surface Pd layer [19], but all measurements under UHV conditions are basically hampered by unknown distributions of carbon among near-surface and deeper bulk regions. Therefore, it is necessary to investigate the Pd catalyst in situ to detect species on and also below the surface that are stable only under steady reaction conditions. X-ray photoelectron spectroscopy (XPS) using tunable synchrotron light is one of the most powerful in situ techniques because it can monitor both the surface and the near-surface regions with high sensitivity, including the possibility of information depth variation.

2. Experimental

Conventionally, XPS is operated under UHV, because the photoelectrons are strongly scattered in a high-pressure gas phase. To overcome these limitations, high-pressure XPS chambers were designed in the late 1970s [22]. Numerous high-pressure XPS experiments have been performed since then [23–25]. The in situ XPS setup used for this study uses differentially pumped electrostatic lenses and allows measurement of the sample in a gaseous environment (batch flow reactor mode) at pressures of up to 1 mbar.

The experiments were performed at beamline U49/2-PGM1 at BESSY in Berlin. The high-pressure XPS setup has been described elsewhere [26]. The photoelectron binding energy (BE) was calibrated with respect to the Fermi edge. The sample, a (111)-oriented Pd single crystal, was mounted on a temperature-controlled heating stage. The temperature was measured by a chromel–alumel thermocouple spot-welded onto the side of the sample. The sample was heated by an IR laser from the rear. The sample cleaning procedures consisted of repeating cycles of Ar^+ sputtering at room and elevated temperature, annealing up to 950 K in UHV, and exposure to O_2, followed by flashing at 950 K for 60 s in UHV. The sample cleanliness was checked by XPS. The Pd(111) single crystal sample was positioned inside a high-pressure cell 2 mm away from a 1-mm aperture, the entrance to a differentially pumped electrostatic lens and to the hemispherical analyzer.

To study the activity, selectivity, and chemical state of the catalyst during ethene oxidation, a reaction mixture of ethene and oxygen (ratio 1:3) was allowed to flow through its reaction chamber. The total flow rate was empirically adjusted for a sufficiently sensitive detection of the reaction products by a QMS, which was supplied with a minor portion of the reaction mixture via a defined capillary leak. In our experimental setup, neither the exact supply rate of the reactants through the leak valves nor the effective pump rate of the reaction chamber could be calibrated with reasonable precision. Thus we need to limit ourselves to the partial pressure data of reactants and products in the reaction chamber under steady reaction conditions, and we cannot quantify turnover rates. The partial pressure data were calculated on the basis of the decrease of the QMS intensities of oxygen ($m/z = 32$) and ethene ($m/z = 27$) and of the increase of CO ($m/z = 28$), water ($m/z = 18$), and CO_2 ($m/z = 44$) induced by the catalytic reaction. The total reactant pressure and the actual partial pressure ratio of ethene and oxygen were measured by an ionization gauge before the onset of the reaction (cold catalyst), thereby accounting for their relative ionization probability. On this basis, the $m/z = 27$ ethene and $m/z = 32$ oxygen QMS signals could be calibrated. Because in our experiment no measurable amounts of molecular reaction products (e.g., acetic acid, acetaldehyde) were detectable, the reaction stoichiometry is limited to the irreversible formation of water, CO, and CO_2:

$$C_2H_4 + (3-x)O_2 \rightarrow (2x)CO + (2-2x)CO_2 + 2H_2O$$
$$\text{with } 0 < x < 1.$$

The known relative detection sensitivity of CO and CO_2 in the QMS was used to determine x from the $m/z = 28$ and $m/z = 44$ signals. Because the mass 28 signal represents a superposition of the ethene and CO molecule ion contributions, at first the appropriate intensity contribution of the ethene-induced $m/z = 28$ signal was subtracted from the total $m/z = 28$ signal, to extract the CO-related contribution. This was done by amplifying the solely ethene-related $m/z = 27$ signal curve, which is not influenced by CO, by the known (separately determined) signal ratio of $m/z = 28$ to $m/z = 27$ for clean ethene, followed by subtraction.

To backcheck the described quantification of the individual partial pressures, the sum of the CO and CO_2 partial pressures was compared with the ethene partial pressure change, and a very good agreement was verified using a factor of 2. Finally, the sum of all product partial pressures (CO, CO_2, and water) equaled the reaction-induced ethene pressure change multiplied by a factor of 4, in accordance with the stoichiometry given above.

The temperature-programmed catalysis experiments involved heating with a linear ramp rate of 10 K/min from 330 to 923 K, holding the temperature at 923 K for 3 min, and cooling, again with a linear ramp of 10 K/min, to 423 K. During this temperature program, the composition of the gas phase was continuously measured with the QMS, and XPS spectra (O1s, C1s, Pd3d region, Fermi edge, and survey spectra, to check for contaminants; photon energy, 650 eV) were continuously recorded. The deconvolution of the $Pd3d_{5/2}$ XP spectra involved an asymmetric Gausso-Lorentzian sum function as described previously [27,28]. Accordingly, the clean Pd(111) $Pd3d_{5/2}$ peak was deconvoluted into two components, an asymmetric bulk and a symmetric surface component [29].

Table 1
Spectral components and parameters of fitting to the $Pd3d_{5/2}$ photoemission peak

XPS peak	Assignment	$Pd3d_{5/2}$ peak		
		BE (eV)	FWHM (eV)	Lorentzian (%)
Pd(111)	Bulk	334.93 ± 0.02	0.75 ± 0.05	25 ± 3
	Surface	334.63 ± 0.04	0.75 ± 0.05	25 ± 3
Adsorbate induced		335.52 ± 0.04	0.75 ± 0.05	25 ± 3
Dissolved carbon induced	Pd_xC_y	335.34 ± 0.03	0.75 ± 0.05	25 ± 3

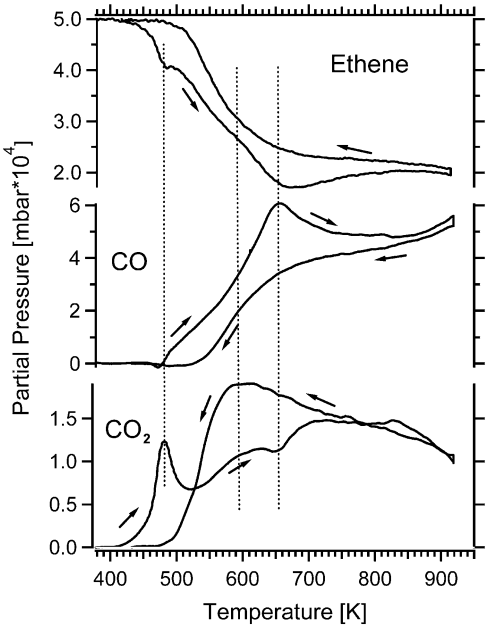

Fig. 1. Partial pressures of CO_2, CO and ethene during the oxidation of ethene plotted against temperature.

The spectra generated by this procedure were optimized by least squares fits to the experimental data with a Shirley-type background considered. The binding energies thus derived (334.93 eV for the bulk and 334.63 for the surface component), were in very good agreement with previous peak fits [29,30], and their shape parameters (FWHM, asymmetry, and mixing factor of the Gausso-Lorentzian sum) were kept within the constrains given in Table 1. To determine the adsorbate and carbon-induced components in the $Pd3d_{5/2}$ spectra, only the binding energies and the peak area were optimized by the fitting procedure. The FWHM and mixing ratio were again kept within the same constraints as the bulk and surface components. Table 1 summarizes the particular components and their fitting parameters.

3. Results

3.1. Heating cycle

Fig. 1 shows the partial pressures of ethene and of the carbon oxide products plotted versus temperature. The traces of CO and CO_2 both show strong hysteresis behavior. Water formation is omitted in Fig. 1, because its partial pressure change closely corresponded to the inverse ethene pressure change multiplied by 2. The top graph shows the partial pressure of ethene and reflects total conversion. The reaction starts at >430 K, a temperature close to results from previous studies on complete thermal ethene decomposition [19]. It was shown that ethene starts to decompose to carbon and hydrogen in the temperature range above 410 K and that C subsurface migration starts above 440 K on both the Pd(111) [19] and Pd(110) surfaces [31]. The initial activity increase exhibits a remarkable "fine structure" as a minimum in the ethene partial pressure evolves at 480 K (left dotted line in Fig. 1) and the selectivity for CO_2 formation is almost 100% (compare also the respective selectivity plot in Fig. 8); that is, CO formation has not yet started. In a small window between 480 and 500 K, ethene conversion stagnates and CO_2 formation slows, reaching a first minimum at 520 K, and the rate of CO formation increases in this range. The catalyst now becomes highly active with respect to CO formation, and both ethene conversion and CO partial pressure reach a peak at 660 K ($p_{CO} = 6 \times 10^{-4}$ mbar), in contrast to CO_2 formation, which shows only a shallow increase up to about 620 K and exhibits a minimum at 660 K (Fig. 1, right dotted line). In general, the low-temperature region (380–660 K) is characterized by a significant activity increase from zero to the maximum value and a dramatic decrease in CO_2 selectivity (given in Fig. 8, derived from the data of Fig. 1) from >90% to ∼20%, and vice versa by a significant increase in CO selectivity from <10% to ∼80%.

From 660 up to 923 K, the activity with respect to ethene conversion remains in a relatively narrow range, and the selectivity changes (CO vs CO_2) are much less pronounced. CO remains the main product at high temperatures (Fig. 8). The CO_2 formation rate (Fig. 1) and selectivity (Fig. 8) increase from 660 to 750 K and then again decrease up to 923 K, as complemented by the inverse trend in CO formation and selectivity, the latter ranging in between 84 and 70% (CO_2 between 15 and 30%).

The same holds for the cooling cycle in between 923 and 700 K. The selectivity pattern and the total activity are close to the values observed during heating; that is, no strong hysteresis effects are observed in this temperature range. The situation changes drastically below 700 K; CO formation diminishes rapidly, but now without passing through a maximum at 660 K, and approaches a zero rate at 520 K. In contrast, the CO_2 rate increases continuously between 923 and 600 K, reaches a pronounced maximum at 600 K (Fig. 1, middle dotted line), and then decreases steeply to approach a zero rate at around 500 K. The-low temperature maximum of CO_2 formation observed during heating at 480 K is missing. The data of Figs. 1 and 8 clearly show pronounced hysteresis of the CO and CO_2 formation rates and selectivities, giving rise to a *selectivity* hysteresis rather than a hysteresis in total activity.

In situ XPS spectra were recorded continuously during the temperature-programmed reaction experiment. Fig. 2 displays the C1s spectral region during the heating cycle. As indicated by the low-temperature spectra (330–461 K), the Pd(111) surface is covered by carbon-containing surface species. The C1s

signal shows a broad peak between 283 and 286 eV lacking analyzable structural features. An adlayer consisting of only ethylidyne (e.g., from ethene adsorbed at 300 K) gives rise to a rather complex spectrum of 4 components in the range of 283.5–285 eV [32]. Moreover ethylidyne should gradually decompose above 350 K toward more dehydrogenated molecular adsorbates (e.g., ethinyl [CCH]), and finally toward atomic carbon [19,33]. Therefore, and also because oxygenated intermediates also may be formed, we consider any meaningful deconvolution and assignment of peak components to known carbonaceous species impossible on the basis of the present XPS data. Only a separate peak with a maximum at 285.65 eV is most likely due to adsorbed CO, corresponding to a C1s signal usually observed at binding energies between 285.53 eV for low CO coverage and 285.80 eV for saturation coverage [34]. There are no hints of more strongly oxygenated carbon species, such as formate or acetate, on the surface causing high BE features above 286 eV [35]. From 461 to 505 K, the C1s spectrum is completely changed. The broad C1s intensity between 283 and 285.5 eV disappears, as does the intensity at 285.65 eV characteristic of adsorbed CO. Instead, a sharp, symmetric single C1s peak (FWHM, 0.4 eV; spectral resolution, ∼0.1 eV) is observed at 284.50 eV, indicating the presence of a single C species. The BE shift relative to adsorbed CO is in good agreement with theoretical results calculated for dissolved carbon atoms [18]. This peak exhibits an approximately constant intensity up to 583 K and vanishes above 677 K.

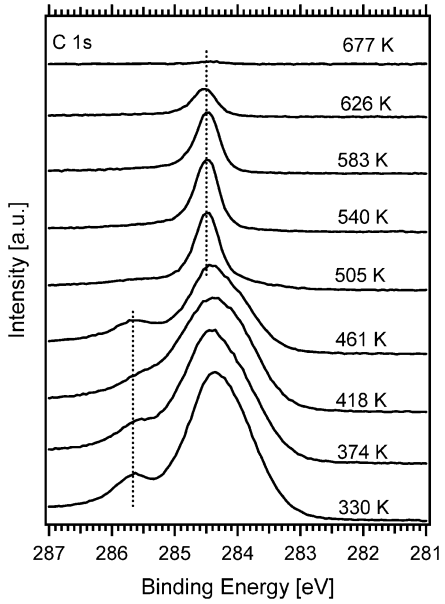

Fig. 2. C1s region recorded during heating from 330 to 677 K. Photon energy 650 eV.

In analogy to the effects observed for the C1s region in Fig. 2, the Pd3d$_{5/2}$ peaks displayed in Fig. 3a show an additional shoulder at the high BE side in between 358 and 444 K, characteristic of an adsorbate covered Pd(111) metal surface [34]. The dotted line indicates the peak position of the Pd bulk component according to [29]. The presence and constant intensity of the bulk Pd component proves that in this temperature range the gas–surface interaction is indeed limited to the surface, as will be shown by the peak deconvolution of Fig. 3b.

A strong change is observed as the temperature becomes higher and CO formation starts (480 K in Fig. 1). The peak maximum shifts from the original bulk Pd position at 334.9 eV up to 335.4 eV, and the peak becomes nearly symmetric. A very similar spectrum persists up to 568 K. At 611 K, the bulk Pd component contributes again more strongly to the spectrum, and above 654 K, the whole spectrum becomes rather characteristic of clean Pd metal (peak maximum again at 334.9 eV) [29]. The assignment of this spectrum to cleaned-off Pd metal is cor-

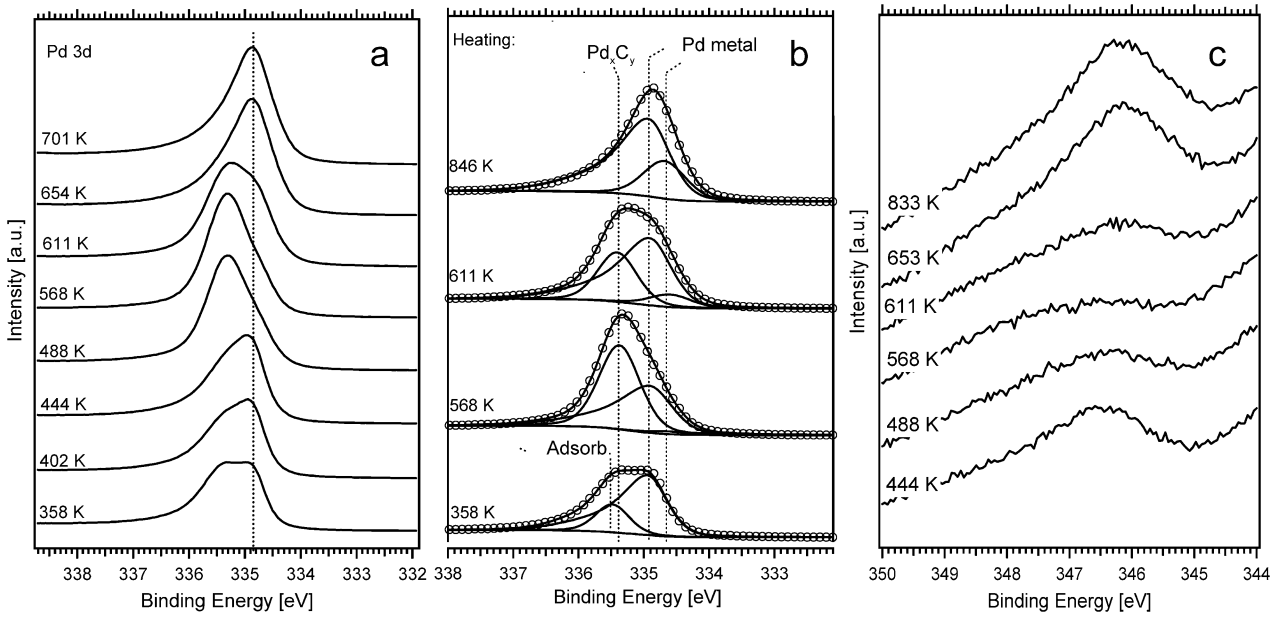

Fig. 3. (a) Pd3d$_{5/2}$ region recorded during heating from 358 K to 701 K. (b) Selected Pd3d$_{5/2}$ photoemission spectra deconvoluted according to Table 1. (c) Palladium plasmon excitation monitored during heating. Photon energy for all spectra 650 eV.

roborated by the absence of measurable C1s and O1s intensity at this temperature (for C1s, see Figs. 2 and 5). The Pd3p/O1s region was monitored throughout the whole TPR experiment, but this spectra series is not shown because it exhibited no detectable O1s intensity contribution. Both O(ad) or surface-oxide related O contributions could be expected and, if present, should be superimposed as a low BE shoulder in the Pd3p–O1s spectral range (BE 528.9 to 530.4 eV) [36]. Our detection limit for such species was deduced from a previous study of Pd(111) oxidation [36] in the same experimental setup under otherwise very similar conditions and is below 0.05 ml. Thus, we conclude that the steady concentration of atomic oxygen species remains below the detection limit over the *whole* temperature range. Moreover, the detection of small amounts of carbon oxygenates, particularly of CO (see CO induced component in the C1s spectra of Figs. 2 and 5 between 330 and 500 K), in the O1s spectra is hampered by the strong overlap with the broad Pd3p emission with a maximum at BE = 532 eV. Therefore, above 650 K, the surface can be considered largely carbon- and oxygen-depleted, and the spectrum of almost-clean Pd(111) is observed.

Selected $Pd3d_{5/2}$ profiles of Fig. 3a were subjected to a standard peak deconvolution using an asymmetric Gausso-Lorentzian sum function applied after Shirley-type background correction, and are shown in Fig. 3b. Table 1 summarizes the BEs of the assignable Pd3d spectral components, on which the deconvolution was based. The experimental data (circles) are reproduced by the sum of three main components, which are assigned to the clean Pd metal surface layer at 334.63 eV, the Pd metal bulk at 334.93 eV, and the Pd component of the electronically altered Pd_xC_y state at 335.34 eV. Only in the 358 K spectrum was an adsorbate-induced component at 335.52 eV added to the deconvolution, in agreement with the presence of hydrocarbon adsorbates and CO (at 285.6 eV in Figs. 2 and 5) at $T < 500$ K. Due to the adsorbate-induced shift of surface Pd, the clean Pd(111) surface component at 334.63 eV is missing at 358 K.

At 568 K, during heating, the bulk Pd component has already decreased, and the Pd_xC_y component has strongly gained in intensity. This trend is reverted again above 611 K, and at 846 K, the presence of a mostly adsorbate-depleted metallic catalyst is indicated by the adequate contribution of the clean surface and bulk Pd metal components [29].

The strong suppression of the Pd metal bulk component at BE = 334.93 eV in the temperature region of 480–660 K indicates major alterations of the electronic state of the Pd(111) near-surface region. In this respect, additional information could be derived from a detailed analysis of the characteristic Pd plasmon loss, which shifts a part of the $Pd3d_{3/2}$ photoelectrons toward higher BE by about 6.5 eV. The corresponding plasmon peak, shown in Fig. 3c, exhibits a maximum intensity at approximately 346.4 eV ($Pd3d_{3/2}$ peak at 340.13 eV). Plasmon shifts of 6–7 eV were reported by Rocca et al. [37,38] and Netzer and El Gomati [39] using angle-resolved EELS. At low temperatures (444 K in Fig. 3c) the still-metallic sample is only adsorbate-covered, and the plasmon peak is clearly visible. The intensity of the loss peak at 444 K in Fig. 3c

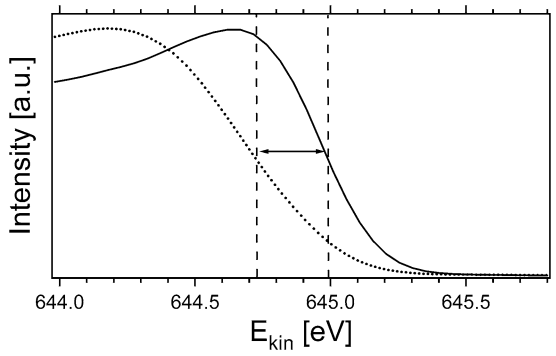

Fig. 4. Fermi edge recorded during heating at 520 (dotted line) and 680 K (solid line).

is slightly lower than that of the adsorbate-depleted metal at $T > 653$ K, most likely due to the adsorbate layer present. This is in agreement with [39], wherein it was shown that, for example, a CO adlayer induces a decrease in the loss intensity. The spectra recorded between 488 and 611 K show that the plasmon vanishes, supporting major changes of the valence band structure of the Pd bulk within the XPS information depth. Above 653 K, the plasmon peak reappears at an intensity ascribed to an adsorbate-depleted metal surface.

Additional support for major electronic changes between 480 and 660 K comes from the observation of a pronounced shift of the highest occupied electronic states toward higher BE with respect to the metal Fermi level by 0.24 eV at 520 K, as shown in Fig. 4. A simply surface-adsorbate covered Pd metal sample would not exhibit such behavior, because the main fraction of photoelectrons originates from the layers below the terminal metal surface layer. The inelastic mean free path of 650 eV electrons is approx. 13 Å, and the fraction of photoelectrons from the first 5 Å is estimated to contribute <40% [40]. We thus conclude that the changes on the catalyst not only affect the top metal layer, but also extend at least over the near-surface region observed by XPS. The perfect reversibility of the observed shift on decay of the carbon-rich surface modification at >660 K proves that this effect exclusively affects the sample near-surface region.

3.2. Cooling cycle

As shown in Fig. 5, during cooling from 923 to 646 K, the C1s intensity remains close to zero, as does the O1s intensity (which is beyond the detection limit at any temperature), thus supporting the presence of a strongly adsorbate-depleted surface. Small amounts of C accumulate at 646 K and below, as indicated by a single small peak at 284.50 eV. This peak quickly gains intensity as the temperature drops below 603 K. At 506 K and below, the spectra develop a shoulder at the low-BE site, likely stemming from carbonaceous species in a low oxidation state. Speculatively, ethylidyne (intensity maximum at 284.0 eV) [32] and more strongly dehydrogenated ethene fragments, such as ethinyl (CCH), could be found [33]. A second peak at 285.65 eV (left dotted line in Fig. 5) appearing at $T < 557$ K is again attributed to CO, in analogy to Fig. 2. The main intensity contribution to the whole spectrum remains that

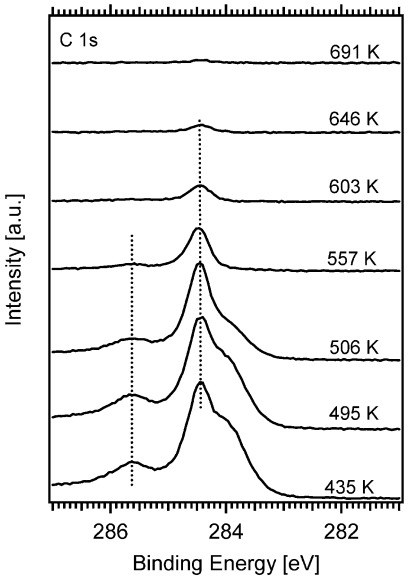

Fig. 5. C1s region recorded during cooling from 691 to 435 K. Photon energy 650 eV.

of the dissolved C component at 284.50 eV over the whole temperature range down to 435 K. This result is in contrast to the 330–461 K heating spectra shown in Fig. 2. During heating, the 284.50 eV component characteristic of dissolved C atoms should start to contribute to the C1s intensity above 480 K, as deduced from the increase of the related Pd_xC_y Pd3d component in Fig. 3a at 488 K.

Complementing the C1s data of Fig. 5, Fig. 6a displays the $Pd3d_{5/2}$ spectral range monitored during cooling. In Fig. 5, the first traces of carbon are visible at 646 K, but the amount of carbon increases substantially at around 557 K. According to this increase in the Pd3d region, a pronounced change of the Pd3d peak shape is also observed at $T < 574$ K. In analogy to the heating spectra (Fig. 3a, between 488 and 611 K), an increased contribution of a component at higher BE and a decrease in the Pd metal bulk component contribute to the change in peak shape. In contrast to the heating cycle, these changes persist down to the lowest temperature (423 K), and the surface does not return into the adsorbate-covered metallic state observed at the beginning of the heating cycle (Fig. 3, $T < 444$ K). This difference is quantified in the selected deconvoluted spectra of the cooling cycle shown in Fig. 6b. At 529 K, the Pd_xC_y component (335.34 eV) is strongly predominant and—although slightly reduced—remains predominant down to the lowest temperature.

On the basis of Figs. 6a and 6b, it is likely that the electronically altered state of the carbon-doped catalyst observed during heating above 480 K (Fig. 3) becomes quenched during the cooling cycle and remains stable down to 400 K. This state is also characterized by the C1s contribution at 284.50 eV, which grows steadily during cooling down to 400 K (Fig. 5).

A more direct proof for the formation of the Pd_xC_y state during cooling below 611 K and its persistence below 480 K can be derived from the changes of the plasmon peak at 346.4 eV shown in Fig. 6c. Whereas the 574 K trace is still characteristic of the metallic state of the catalyst, at 529 K, complete extinction of the plasmon excitation is observed. In contrast to the heating cycle (Fig. 3c, 444 K), the plasmon peak cannot be observed at the lowest temperature (Fig. 6c, 423 K); that is, the catalyst remains in the Pd_xC_y state during cooling.

To prove the extended bulk nature of the Pd_xC_y species, depth profiling by varying the incident photon energy was performed at a constant temperature of 488 K (Fig. 7). Because the mean free path of an electron in a solid depends on its kinetic energy (KE), the escape depth of the photoelectrons varies with the incident photon energy (h), according to $KE = h - BE - \Phi$ (where Φ is the work function). We recorded spectra at four different incident photon energies: 460, 590, 720, and 910 eV. These correspond to inelastic mean free path lengths of 5, 7, 9, and 12 Å (assuming that palladium remains the predominant constituent in the near-surface region) [40]. From Fig. 7, it is obvious that the relative contribution of the bulk Pd metal and the Pd_xC_y components changes little with the information depth. The incorporated carbon not only affects the first layer of Pd(111), but also extends at least over 12 Å, and we also may deduce that the concentration of carbon in Pd_xC_y decreases slightly within deeper layers, as suggested by the slight decrease in the Pd_xC_y to Pd bulk ratio with increasing IMFP. This result is important in view of a recent XRD study [41] analyzing the chemical state of alumina-supported palladium catalysts (1 and 3% Pd) during the oxidation of unsaturated hydrocarbons under O_2 substoichiometric conditions. The formation of a new crystallographic phase with a larger lattice constant than that of clean Pd metal has been reported previously [41]; it was denoted as "PdX," where X represents oxygen. Lacking information about the chemical composition of this phase, the phase change was attributed to the formation of a Pd-oxygen compound, but on the basis of our work, we suggest instead Pd modified by a considerable carbon loading.

4. Discussion

Fig. 8 shows the possible origin of the observed selectivity hysteresis on the basis of the intensity changes of the Pd3d Pd_xC_y component at 335.34 eV, representing the electronically altered state of the catalyst induced by the high subsurface/dissolved carbon loading. The selectivities given in the lower graph of Fig. 8 are based on the fraction of the partial pressures with respect to the carbon oxide total pressure $p(CO)/(p(CO) + p(CO_2)) \times 100\%$ and $p(CO_2)/(p(CO) + p(CO_2)) \times 100\%$. This plot had to be limited to the temperature range, in which the overall reaction rate (ethene consumption) is already high enough. If the partial pressures of CO and CO_2 are very low (i.e., close to the baseline) at the lowest temperatures, then the relative error and the noise are too high to allow extraction of any useful value for the selectivity.

4.1. Heating cycle

For clarity, three distinct temperature regions are discussed:

1) Low-temperature region (up to 480 K). A Pd(111) metal surface covered by an adsorbate layer containing CO is

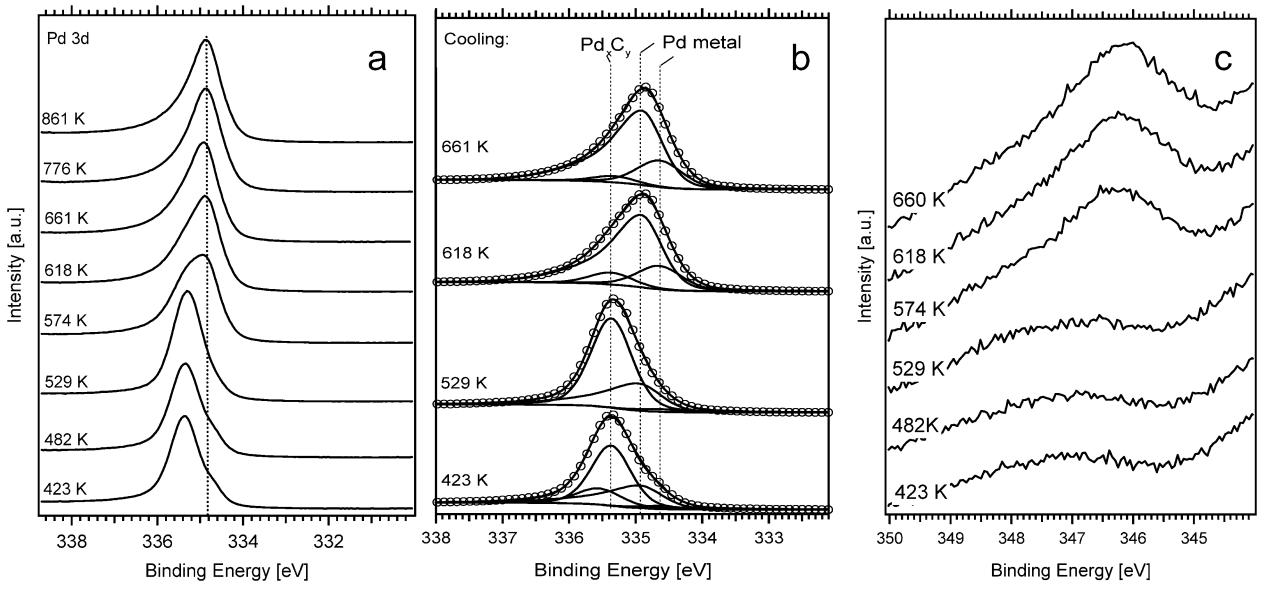

Fig. 6. (a) Pd3d$_{5/2}$ region recorded during cooling from 861 to 423 K. (b) Selected Pd3d$_{5/2}$ photoemission spectra deconvoluted according to Table 1. (c) Palladium plasmon excitation monitored during cooling. Photon energy for all spectra 650 eV.

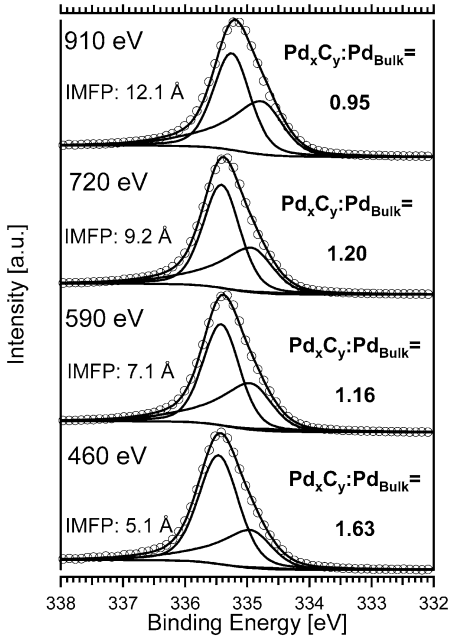

Fig. 7. Pd3d$_{5/2}$ photoemission spectra recorded at 473 K and at the indicated photon energies. The information depth of the emitted electrons (inelastic mean free path) was calculated according to [40].

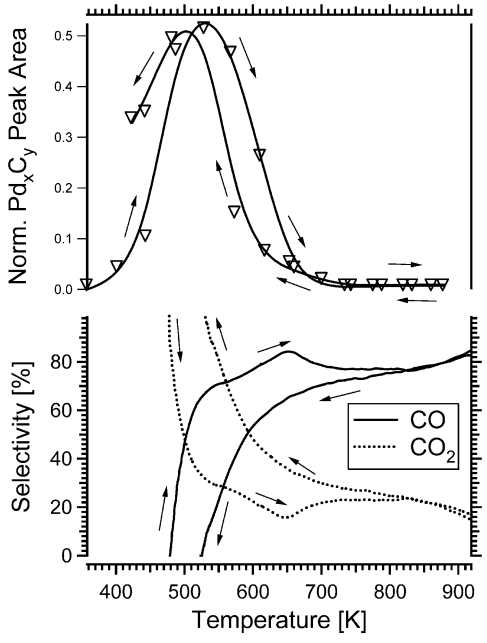

Fig. 8. Top graph: temperature hysteresis of the dissolved carbon Pd$_x$C$_y$ (335.34 eV) component. Bottom graph: temperature hysteresis of the fractional contribution (in %) of p(CO) (solid line) and p(CO$_2$) (dashed line) to the total pressure of the carbon oxide reaction products p(CO) + p(CO$_2$).

present, the Pd3d Pd$_x$C$_y$ intensity remains low (we previously showed that ethene decomposition toward carbon becomes rapid at $T > 410$ K and migration of carbon into the bulk at >480 K [19]) and the main reaction product is CO_2. Between 461 and 505 K, the CO C1s signal at 285.4 eV (Fig. 2) vanishes, probably due to the increasing rate of the CO–oxygen reaction reflected by the increased CO_2 production (maximum at 480 K; Fig. 1). At ∼480 K the CO desorption rate from metallic Pd(111) is still relatively low [42,43], and the lifetime of the chemisorbed CO is probably sufficiently high to permit oxidization to CO_2 before desorption, according to a Langmuir–Hinshelwood reaction mechanism on the metal between O(ads) and CO(ads).

2) 480–660 K. According to previous work [19], in this temperature region the subsurface migration of surface-adsorbed carbon accelerates steeply. The Pd3d Pd$_x$C$_y$ intensity passes through a pronounced maximum at 520 K. On the dissolved carbon phase, CO becomes the main reaction product and is formed at a sharply increasing rate, meaning that the oxidation mechanism on Pd$_x$C$_y$ strongly boosts CO formation (from <10 to >80%) and suppresses

CO_2 formation (from >90 to <20%; Fig. 8). For a tentative explanation, we may consider the too-short lifetime of CO on the Pd_xC_y phase to allow oxidization by adjacent O atoms, which also may be quickly consumed by this extremely carbon-rich catalyst environment. This may lead to suppression of the secondary CO oxidation toward CO_2. Generally spoken, it is very likely that CO_2 formation from C and O proceeds via intermediate CO, rather than through a single three-body microkinetic process.

Recent work on CO adsorption on carbon-modified Rh(100) by Nieskens et al. [44] has revealed that both surface and subsurface carbon greatly influence CO adsorption. C(sub) shifts the average desorption temperature of CO to lower values, which would eventually result in a reduced CO equilibrium coverage (and microscopically in a reduced average CO lifetime) at, for example, 500 K.

3) 660–923 K. Beyond the decomposition limit of the dissolved carbon phase the $Pd3d_{5/2}$ spectrum becomes characteristic of an adsorbate-depleted Pd(111) metal surface. This transition is accompanied by partial reversal of selectivity toward CO_2 up to 750 K (from <20 to ∼25%). Above 750 K, again a trend toward more CO (finally 85% CO vs 15% CO_2 at 923 K) is obvious. As was concluded from the C1s and O1s spectra, in this temperature region both the C(ads) and O(ads) concentrations are below the detection limit, so it was not possible to trace the origin of these trends spectroscopically. A simplified but rather general concept could again be based on the lifetime ratio of adsorbed CO and oxygen as a function of temperature on the purely metallic surface. This concept is also implied by the QMS data in Fig. 1, which show no strong hysteresis in the high-temperature region (>700 K); that is, the strong hysteresis effects at temperatures below 700 K are clearly related to the formation and decay of the dissolved carbon phase. From TPD studies of oxygen desorption from Pd(111) [45,46], it is known that chemisorbed oxygen starts to desorb at around 650 K and reaches a maximum at ∼720 K. This opens an additional reaction channel to decrease the (unmeasurably low) steady oxygen surface coverage at around 800 K and may explain the gradual selectivity shift toward CO above 750 K.

4.2. Cooling cycle

Down to ∼720 K, only minor hysteresis is observed, and the arguments presented earlier for the heating cycle above ∼720 K hold. In contrast to the heating cycle, below 720 K a general trend toward more CO_2 (Fig. 8, strong CO_2 maximum at 600 K in Fig. 1) and less CO is clearly observed. This trend is related to the delayed formation of the Pd_xC_y phase at $T \sim 550$ K during cooling (Fig. 8). An increasing lifetime of CO(ads) from 720 to <600 K on the predominantly metallic surface may explain the significant increase in CO_2 formation rate and selectivity at least down to ∼550 K. During heating in the same temperature region, the dissolved carbon state of the catalyst was mainly present, leading to preferential CO formation. The Pd_xC_y intensity reaches its maximum during cooling at <500 K, but at this temperature the reaction rate already approaches zero, as can be deduced from Fig. 1. Therefore it is likely that the Pd_xC_y phase is formed at a too low a temperature to contribute substantially to the reaction rate, and the selectivity pattern of the metallic surface is predominant.

5. Conclusion

Ethene oxidation is catalyzed by both the metallic and the dissolved carbon (electronically altered) phase, which preferentially catalyzes CO formation. The observed selectivity hysteresis is a consequence of the delayed buildup of this phase during cooling. Two main reasons for the high selectivity on Pd_xC_y toward CO may be considered: (1) Because reactive C atoms are ubiquitous in the dissolved carbon state of the catalyst, the steady coverage of adsorbed oxygen may be rather low, and (2) a reduced lifetime of CO on the electronically altered surface may specifically favor the CO desorption channel.

Because CO is already a “partial” oxidation product, the importance of the carbon-loaded Pd catalyst for partial oxidation processes is supported (although no molecular reaction products, such as acetic acid or acetaldehyde, could be quantified in this study for experimental reasons). In this respect, the particular importance of an oxygen-depleted but carbon-enriched catalyst, which remains in a highly reduced stated despite the relatively high partial pressure of oxygen, may be rather spotted in the suppression of ethene dissociative adsorption.

Acknowledgments

This work was supported by the European Community Research Infrastructure Action under the FP6 Structuring the European Research Area Programme (through the Integrated Infrastructure Initiative Integrating Activity on Synchrotron and Free Electron Laser Science [Contract R II 3-CT-2004-506008]). The work was also supported by Enterprise Ireland through the International Collaboration Programme (IC/2004/099). D.Z. received a research scholarship from the Foundation of the University of Limerick. H.G. acknowledges a grant from the Max Planck Society. The authors thank the BESSY staff for their support during the beamtime.

References

[1] A.K. Datye, J. Bravo, T.R. Nelson, P. Atanasova, M. Lyubovsky, L. Pfefferle, Appl. Catal. A 198 (2000) 179–196.
[2] R.J. Farrauto, M.C. Hobson, T. Kennelly, E.M. Waterman, Appl. Catal. A 81 (1992) 227–237.
[3] P. Salomonsson, S. Johansson, B. Kasemo, Catal. Lett. 33 (1995) 1.
[4] G.B. Hoflund, H.A.E. Hagelin, J.F. Weaver, G.N. Salaita, Appl. Surf. Sci. 205 (2003) 102–112.
[5] W. Unterberger, H. Gabasch, K. Hayek, B. Klötzer, Catal. Lett. 104 (2005) 1–8.
[6] H.R. Gerberich, N.W. Cant, W.K. Hall, J. Catal. 16 (1970) 204–219.
[7] J. Xie, Q. Zhang, K.T. Chuang, Catal. Lett. 93 (2004) 181–184.
[8] B. Samanos, P. Boutry, R. Montarnal, J. Catal. 23 (1971) 19–30.
[9] Y.F. Han, D. Kumar, D.W. Goodman, J. Catal. 230 (2005) 353–358.
[10] Y.F. Han, D. Kumar, C. Sivadinarayana, A. Clearfield, D.W. Goodman, Catal. Lett. 94 (2004) 131–134.

[11] D. Stacchiola, F. Calaza, L. Burkholder, W.T. Tysoe, J. Am. Chem. Soc. 126 (2004) 15384–15385.
[12] M. Bowker, C. Morgan, Catal. Lett. 98 (2004) 67.
[13] M. Morkel, G. Rupprechter, H.-J. Freund, Surf. Sci. Lett. 588 (2005) L209.
[14] S.B. Ziemecki, G.A. Jones, D.G. Swartzfager, R.L. Harlow, J. Faber Jr., J. Am. Chem. Soc. 107 (1985) 4547.
[15] R.H. Siller, W.A. Oates, R.B. McLellan, J. Less-Common Met. 16 (1968) 71.
[16] Z. Paál, U. Wild, R. Schlögl, Phys. Chem. Chem. Phys. 3 (2001) 4644.
[17] M. Todorova, W.X. Li, M.V. Ganduglia-Pirovano, C. Stampfl, K. Reuter, M. Scheffler, Phys. Rev. Lett. 89 (2002) 096103/1–096103/4.
[18] I.V. Yudanov, K.M. Neyman, N. Rösch, Phys. Chem. Chem. Phys. 6 (2004) 116–123.
[19] H. Gabasch, K. Hayek, B. Klötzer, A. Knop-Gericke, R. Schlögl, J. Phys. Chem. B 110 (2006) 4947–4952.
[20] M.K. Rose, A. Borg, T. Mitsui, D.F. Ogletree, M. Salmeron, J. Chem. Phys. 115 (2001) 10927–10934.
[21] L. Gracia, M. Calatayud, J. Andres, C. Minot, M. Salmeron, Phys. Rev. B 71 (2005) 033407/1–033407/4.
[22] R.W. Joiner, M.W. Roberts, Chem. Phys. Lett. 60 (1979) 459.
[23] V.I. Bukhtiyarov, V.V. Kaichev, I.P. Prosvirin, Top. Catal. 32 (2005) 3–15.
[24] R. Würz, M. Rusu, T. Schedel-Niedrig, M.C. Lux-Steiner, H. Bluhm, M. Hävecker, E. Kleimenov, A. Knop-Gericke, R. Schlögl, Surf. Sci. 580 (2005) 80–94.
[25] R. Schlögl, D. Teschner, A. Knop-Gericke, M. Hävecker, E. Kleimenov, D. Su, in: Abstracts of Papers, 228th ACS National Meeting, Philadelphia, PA, US, August 22–26, 2004, COLL-194.
[26] H. Bluhm, M. Hävecker, A. Knop-Gericke, E. Kleimenov, R. Schlögl, D. Teschner, V.I. Bukhtiyarov, D.F. Ogletree, M. Salmeron, J. Phys. Chem. B 108 (2004) 14340–14347.
[27] D. Teschner, A. Pestryakov, E. Kleimenov, M. Hävecker, H. Bluhm, H. Sauer, A. Knop-Gericke, R. Schlögl, J. Catal. 230 (2005) 186–194.
[28] A. Bayer, K. Flechtner, R. Denecke, H.-P. Steinrück, K.M. Neyman, N. Rösch, Surf. Sci. 600 (2005) 78–94.
[29] J.N. Andersen, D. Hennig, E. Lundgren, M. Methfessel, R. Nyholm, M. Scheffler, Phys. Rev. B 50 (1994) 17525–17533.
[30] F.P. Leisenberger, G. Koller, M. Sock, S. Surnev, M.G. Ramsey, F.P. Netzer, B. Klötzer, K. Hayek, Surf. Sci. 445 (2000) 380–393.
[31] M. Bowker, C. Morgan, N. Perkins, R. Holroyd, E. Fourre, F. Grillo, A. MacDowall, J. Phys. Chem. B 109 (2005) 2377–2386.
[32] M. Sock, A. Eichler, S. Surnev, J.N. Andersen, B. Klötzer, K. Hayek, M.G. Ramsey, F.P. Netzer, Surf. Sci. 545 (2003) 122–136.
[33] M. Nishijima, J. Yoshinobu, T. Sekitani, M. Onchi, J. Chem. Phys. 90 (1989) 5114–5127.
[34] S. Surnev, M. Sock, M.G. Ramsey, F.P. Netzer, M. Wiklund, M. Borg, J.N. Andersen, Surf. Sci. 470 (2000) 171–185.
[35] R.D. Haley, M.S. Tikhov, R.M. Lambert, Catal. Lett. 76 (2001) 125–130.
[36] D. Zemlyanov, B. Aszalos-Kiss, E. Kleimenov, D. Teschner, S. Zafeiratos, M. Hävecker, A. Knop-Gericke, R. Schlögl, H. Gabasch, W. Unterberger, K. Hayek, B. Klötzer, Surf. Sci. 600 (2006) 983–994.
[37] M. Rocca, F. Moresco, Prog. Surf. Sci. 53 (1997) 331–340.
[38] M. Rocca, S. Lizzit, B. Brena, G. Cautero, G. Comelli, G. Paolucci, J. Phys. B 7 (1995) L611–L618.
[39] F.P. Netzer, M.M. El Gomati, Surf. Sci. 124 (1983) 26–38.
[40] S. Tanuma, C.J. Powell, D.R. Penn, Surf. Interface Anal. 17 (1991) 911–926.
[41] Z. Ferhat-Hamida, J. Barbier Jr., S. Labruquere, D. Duprez, Appl. Catal. B 29 (2001) 195–205.
[42] B. Klötzer, W. Unterberger, K. Hayek, Surf. Sci. 532 (2003) 142.
[43] X. Guo, J.T. Yates Jr., J. Chem. Phys. 90 (1989) 6761–6766.
[44] D.L.S. Nieskens, M.M.M. Jansen, A.P. van Bavel, D. Curulla-Ferre, J.W. Niemantsverdriet, Phys. Chem. Chem. Phys. 8 (2006) 624–632.
[45] B. Klötzer, K. Hayek, C. Konvicka, E. Lundgren, P. Varga, Surf. Sci. 482–485 (2001) 237–242.
[46] H. Gabasch, W. Unterberger, K. Hayek, B. Klötzer, G. Kresse, C. Klein, M. Schmid, P. Varga, Surf. Sci. 600 (2005) 205–218.